THESIS FOR THE DEGREE OF LICENTIATE OF ENGINEERING

Electromagnetic modeling and design of medical implants and devices

by

OSKAR TALCOTH

CHALMERS

Department of Signals and Systems
CHALMERS UNIVERSITY OF TECHNOLOGY
Göteborg, Sweden 2011

Göteborg 2011

Electromagnetic modeling and design
of medical implants and devices
OSKAR TALCOTH

This thesis has been prepared using LaTeX.

Copyright © OSKAR TALCOTH, 2011.
All rights reserved.

Licentiatavhandling vid Chalmers Tekniska Högskola
Ny serie nr R016/2011
ISSN 1403-266X

Department of Signals and Systems
Biomedical Electromagnetics Group
Chalmers University of Technology
SE-412 96 Göteborg, Sweden

Phone: +46 (0)31 772 5186
E-mail: `oskar.talcoth@chalmers.se`

Front cover: Photo and mesh of the distal end of a clinical pacemaker lead.

Printed by Chalmers Reproservice
Göteborg, Sweden, November 2011

If it gets difficult in places, well,
that's life - there is no other way.
Richard P. Feynman

Abstract

This thesis covers two topics in biomedical electromagnetics: pacemaker lead heating in magnetic resonance imaging (MRI) and optimization of sensor positions in magnetic tracking.

The electromagnetic part of pacemaker lead heating during MRI is a resonant phenomenon which is complicated by, among other factors, the wide range of length scales involved in the problem. In this work, the multi-scale part of the problem is taken into special consideration during the modeling process. The model incorporates a radio frequency coil, a human body phantom, and a highly detailed model of a pacemaker system with a bipolar lead that features helix-shaped conductors.

Several configurations of pacemaker systems exposed to MRI are modeled and the results clearly show the importance of detailed lead modeling. Furthermore, modeling of resonant structures is investigated by a comparison between different modeling techniques. In addition, a meshing scheme for thin-wire approximations of helices is proposed, evaluated, and found to have improved convergence properties as compared to the conventional meshing approach.

In recent years, magnetic tracking has been applied in many biomedical settings due to the transparency of the human body to low-frequency magnetic fields. In this work, the sensor positions of a magnetic tracking system are optimized by exploiting an analytical model where the transmitting and sensing coils of the system are approximated by magnetic dipoles.

In order to compare different sensor array layouts, two performance measures based on the Fisher information matrix are discussed and compared for the optimization of the sensor positions of a circular sensor array. Furthermore, the sensor positioning problem is formulated as an optimization problem which is cast as a sensor selection problem. The sensor selection problem is solved for a planar sensor array by the application of a convex relaxation. Several transmitter positions are considered and general results are established for the dependence of the optimal sensor positions on the transmitter's position and orientation.

Preface

This thesis is in partial fulfillment of the requirements for the degree of Licentiate of Engineering at Chalmers University of Technology, Göteborg, Sweden.

The work has been performed in the Biomedical Electromagnetics Group, Department of Signals and Systems at Chalmers between Aug. 2008 and Nov. 2011 under the supervision of Professor Mikael Persson, Associate Professor Thomas Rylander and Assistant Professor Hoi-Shun Lui. Prof. Persson also acts as examiner of the thesis. In addition to the supervisors, Dr. Tonny Rubæk has been involved in this work.

This work has been supported in part by The Swedish Governmental Agency for Innovation Systems (VINNOVA) within the VINN Excellence Center Chase. Being a part of Chase, the project has been performed in collaboration with industry, namely Micropos Medical in Göteborg and St. Jude Medical in Järfälla, Sweden. At Micropos Medical, Andreas Bergqvist, Tomas Gustafsson, Roman Iustin, Johan Linder, Sören Schindler, and Hanna Syrén have been involved in the project. St. Jude Medical has been represented by Kenneth Dahlberg, Åke Sivard, Niklas Sköldengen, Hans Strandberg, and Michael Wang.

Related to this work are the two master thesis projects performed by Johan Gustafsson and Albert Oskarsson as part of their studies at Chalmers.

The work has been supported by the Swedish National Graduate School in Scientific Computing. Computations were mainly performed on C3SE computing resources at Chalmers.

List of Publications

This thesis is based on the work contained in the following papers, referred to in the text by their boldface Roman numerals.

I. "Monolithic Multi-Scale Modeling of MR-Induced Pacemaker Lead Heating",
O. Talcoth, T. Rylander, H.S. Lui and M. Persson,
Proceedings of the International Conference on Electromagnetics in Advanced Applications (ICEAA), 2011, pp. 599-602, Torino, Italy, 12-16 Sept. 2011.

II. "Electromagnetic modeling of pacemaker lead heating during MRI",
O. Talcoth and T. Rylander,
Technical report R014/2011, ISSN 1403-266X, Department of Signals and Systems, Chalmers University of Technology, Göteborg, Sweden, Nov. 2011.

III. "Optimization of sensor positions in magnetic tracking",
O. Talcoth and T. Rylander,
Technical report R015/2011, ISSN 1403-266X, Department of Signals and Systems, Chalmers University of Technology, Göteborg, Sweden, Nov. 2011.

Other related publications by the author not included in this thesis:

1. O. Talcoth, H.S. Lui and M. Persson, "Simulation of MRI-induced heating of implanted pacemaker leads", *Proceedings of Medicinteknikdagarna 2009*, Västerås, Sweden, Sept. 28-29, 2009.

2. O. Talcoth, T. Rylander, H.S. Lui and M. Persson, "Optimization of sensor placement in magnetic tracking", *Proceedings of Medicinteknikdagarna 2010*, Umeå, Sweden, Oct. 6-7, 2010.

3. O. Talcoth, T. Rylander, H.S. Lui and M. Persson, "MR-induced heating of pacemaker leads: Modeling and simulations", *Proceedings of Medicinteknikdagarna 2010*, Umeå, Sweden, Oct. 6-7, 2010.

4. P. Damsgaard Jensen, T. Rubæk, O. Talcoth and J.J. Mohr, "Investigation of the Influence of Problem Formulation and Parameter Scaling in Non-Linear Microwave Tomography", submitted to *International Journal of Biomedical Imaging*, Sept. 2011.

5. O. Talcoth, T. Rylander, H.S. Lui and M. Persson, "Optimal measurements in magnetic tracking for organ-positioning during radiotherapy", *Proceedings of Medicinteknikdagarna 2011*, Linköping, Sweden, Oct. 11-12, 2011.

6. O. Talcoth, T. Rylander, H.S. Lui and M. Persson, "MR-induced heating of pacemaker leads: A parameter study of contributing factors based on multi-scale modeling", *Proceedings of Medicinteknikdagarna 2011*, Linköping, Sweden, Oct. 11-12, 2011.

Acknowledgments

I would like to express my gratitude to the following:

Prof. Mikael Persson, *Chalmers University of Technology*,
Dr. Hoi-Shun Lui, *Chalmers*,
Dr. Tonny Rubæk, *Chalmers*,
Roman Iustin and colleagues, *Micropos Medical*,
Michael Wang and colleagues, *St. Jude Medical*,
Dr. Daniel Nilsson, *C3SE, Chalmers*,
Dr. Erik Abenius, *Efield*,
Johan Gustafsson, *Cochlear, Chalmers*,
Albert Oskarsson, *Berdiz Consulting, Chalmers*,
Kjell Attback, *SAAB Defense, Volvo Cars*,
Colleagues and students, *Dept. of Signals and Systems, Chalmers.*

In particular, I would like to acknowledge Dr. Thomas Rylander, *Chalmers*, for his outstanding generosity, dedication, and guidance.

I am also greatly indebted to my family and friends for their invaluable support.

Oskar Talcoth
Göteborg, Nov. 25, 2011

Contents

Abstract **i**

Preface **iii**

List of Publications **v**

Acknowledgments **vii**

Contents **ix**

Part I: Introduction **1**

1 Introduction **3**
- 1.1 Electromagnetics in biomedical engineering 3
- 1.2 Electromagnetic modeling 4
- 1.3 Computational electromagnetics 5
  - 1.3.1 FDTD 5
  - 1.3.2 FEM 5
  - 1.3.3 MoM 6
  - 1.3.4 Errors and validation 6
- 1.4 Overview of the thesis 7

2 Pacemaker lead heating during MRI **9**
- 2.1 Introduction to MR safety 9
  - 2.1.1 Static field 9
  - 2.1.2 Gradient fields 10
  - 2.1.3 RF field 10
- 2.2 Pacemaker safety in MRI 11

2.2.1 Case reports on deaths 11
2.2.2 MR safe pacemaker design 12
2.3 Pacemaker lead heating 13
2.3.1 Mechanism 13
2.3.2 Influencing factors 13
2.3.3 Impact of design parameters 14
2.3.4 Measurements and countermeasures 17

3 Optimization of sensor positions in magnetic tracking 19
3.1 Biomedical applications of magnetic tracking 19
3.2 Positioning procedure 20
3.3 Optimization of sensor positions 20
3.3.1 Performance measures 20
3.3.2 Example problem 22

4 Aim and overview of this work 25
4.1 Electromagnetic modeling of pacemaker lead heating during MRI 25
4.2 Optimization of sensor positions in magnetic tracking 26

References 29

Part II: Publications 35

Paper I: Monolithic Multi-Scale Modeling of MR-Induced Pacemaker Lead Heating

Paper II: Electromagnetic modeling of pacemaker lead heating during MRI

Paper III: Optimization of sensor positions in magnetic tracking

Part I
Introduction

Chapter 1

Introduction

1.1 Electromagnetics in biomedical engineering

Several vital physical processes in the human body can be described with electromagnetics. Most of these processes are related to the nervous system, e.g. muscle stimulation, conduction of nerve signals, and detection of light falling on the retina.

As a consequence, numerous electromagnetic techniques are used in biomedical engineering for both diagnostic and therapeutic purposes. Activity of the nervous system can for example be monitored with electroencephalography (EEG) and magnetoencephalography (MEG) for brain studies. Electrocardiography (ECG/EKG) is used for investigations of the electric activity of the heart whereas microneurography enables observations of individual nerves. Very low frequencies are employed by the abovementioned techniques due to the chemical nature of nerve signal conduction.

Measurements of the human body's response to external electromagnetic fields is also fruitful. At very high frequencies, X-rays are used to image electron density. Both projection and tomographic images (computed tomography, CT) can be obtained. Magnetic resonance imaging (MRI) constitutes the imaging modality of choice for imaging of soft tissues. It exploits static, low frequency and radio frequency (RF) magnetic fields to generate images of the density of single protons (^{1}H) which are mainly found as part of water molecules in the body. The dielectric properties of the tissues in the human body can be imaged by impedance tomography at low frequencies and microwave tomography at microwave frequencies. Furthermore, microwave-based systems are investigated for stroke detection and classification.

There are also electromagnetic treatment modalities. Medical devices such as pacemakers and deep brain stimulation devices (DBS) operate at very low frequencies and are commonly used for treatment of different cardiac and nervous disorders. At low frequencies, magnetic tracking systems have been introduced for positioning purposes. Radio frequency fields are used by RF ablation devices to destroy non-wanted tissue. In the microwave part of the electromagnetic spectrum, chemo- and radiotherapy of cancer tumors can be enhanced by microwave induced hyperthermia. Optical techniques, such as lasers, play an important role in, for example, eye surgery. At very high frequencies, ionizing gamma rays are used for radiotherapy of cancer tumors.

Clearly, electromagnetics is an increasingly important part of contemporary healthcare. To further improve performance of existing techniques and to develop new techniques, electromagnetic modeling is essential.

1.2 Electromagnetic modeling

A mathematical model serves to describe a system with mathematical concepts and language. The act of creating such models is usually referred to as mathematical modeling or simply modeling. Modeling is one of the corner stones of modern science by enabling analysis, simulation and prediction of the system at hand. For example, physical laws are models that, in general, have been inferred from and validated against experiments and measurements. In this thesis, we study electromagnetic phenomena modeled by Maxwell's equations.

Since Maxwell's equations normally are stated in differential or integral form, electromagnetic models are often constituted by these types of equations where one or several unknowns are sought for. Solving the equations can in particular cases be achieved by analytical methods but in most real-life cases numerical techniques have to be exploited. These techniques have grown in popularity and applicability during recent years fueled by the rapid development of computers with their, so far, continuous increase in computing power. Numerical modeling techniques are becoming cheaper and quicker than large measurement campaigns. Furthermore, modeling may be the only alternative in situations where measurements are deemed impossible. For example, measurements in the human body might be feasible but at a great risk to the patient.

1.3 Computational electromagnetics

There are several numerical techniques which are commonly used in solving electromagnetic problems. These techniques all rely on approximations of the problem to solve. The exploited approximations make a specific technique better suited for a certain group of problems. However, no numerical technique is superior to the others for all possible problems. Choosing the proper numerical technique is one important part of the modeling process, which also can affect the modeling in itself.

Having chosen which numerical technique to use, there can still be more approximations available that can lower the computational cost at the price of reduced accuracy. This trade-off between accuracy and computational cost is ever-present in numerical modeling.

Below, the three most common computational techniques for electromagnetic problems are presented and compared, namely the finite-difference time-domain method (FDTD), the finite element method (FEM), and the method of moments (MoM). An introduction to these techniques is given in the monograph by Bondeson et al. [1].

1.3.1 FDTD

The finite-difference time-domain method exploits Maxwell's equations on differential form. The differential operators are approximated with finite differences on a staggered Cartesian grid of the computational volume. A leap-frog scheme is used for the time-stepping. The method is well-suited for heterogeneous media and can quite easily be parallelized for GPU computations (in comparison with FEM and MoM). However, due to the Cartesian grid, complex geometries with curved boundaries are challenging for FDTD. See Yee [2] and Taflove [3] for more information on FDTD.

1.3.2 FEM

The finite element method also exploits the differential form of Maxwell's equations. In contrast to FDTD, FEM approximates the solution instead of the operators. The computational volume is discretized with elements that can have different shapes (tetrahedra, hexahedra, etc.) and, therefore, complex geometries and heterogeneous media can be handled well. Since the FEM involves the solution of a large system of linear equations, the computational cost can be significantly higher for FEM than for FDTD for certain problems. More information on FEM can be found in the works by Nédélec [4], Peterson et al. [5], and Jin [6].

1.3.3 MoM

In contrast to FDTD and FEM, the method of moments exploits Maxwell's equations on integral form. Only boundaries between different media need to be discretized, which makes MoM superior to FDTD and FEM for problems with few media, e.g. a metal object in free space. The MoM is used in papers **I** and **II**.

The MoM exploits the so-called Green's function which in this context describes the electromagnetic fields from a point source. The field generated by sources on a boundary between two different media is obtained by the evaluation of a superposition integral that sums the field contributions from all point sources on the boundary. The distribution of sources on the boundary is found by imposing that the boundary constraints must be fulfilled, e.g. the part of the electric field tangential to the surface of a perfect electric conductor must be zero. A finite element approach with suitable basis functions turns the problem into a system of linear equations $\mathbf{ZI} = \mathbf{E}_{\text{incident}}$ which can be solved for the induced currents, $\mathbf{I}$. The off-diagonal terms in the impedance matrix, $\mathbf{Z}$, describe the interaction between currents represented by different basis functions. For some problems, like the problem in paper **III**, these interactions can be neglected and the problem reduces to a much simpler one.

More information on the MoM can be found in the monograph by Peterson et al. [5].

1.3.4 Errors and validation

Discretization errors, extrapolation and convergence

One of the approximations exploited by numerical techniques is that the original electromagnetic problem, which is continuous in time and space, is discretized. This approximation comes with an associated discretization error. For a well-designed numerical technique, the discretization error decreases in a well-behaved way (linear, quadratic,...) when the discretization is refined. This permits the discretization error to be quantified and controlled by the use of a so-called mesh convergence study where the same problem is solved with a successively finer discretization. Extrapolation techniques can be used to extrapolate the results in the convergence study to zero cell size. However, as a mesh refinement comes at the cost of a larger problem, convergence studies may be intractable for complex problems if, for example, all computational resources are consumed already at the coarsest discretization. An introduction to convergence studies is given in the monograph by Bondeson et al. [1] and an example of such a study can be found in paper **I**.

Validation

Validation of the mathematical model and the possible approximations exploited during its solution can be performed in several ways. To assess the validity of approximations, these can be checked when a solution has been obtained. An approximation that leads to a simplified problem may be compared to the solution of the same problem without the simplification, should the non-simplified problem be solvable. The latter approach is exploited in paper **II**.

A popular means for validation is comparison with measurements. Within the measurement accuracy, the measurements include all relevant factors present in the problem. However, unwanted factors may also affect the measurement results if the measurement setup is not properly designed. Moreover, a significant difficulty is that the same situation must be measured and modeled for the comparison to be meaningful. Uncertainties in dimensions, positions, material properties etc. might give large discrepancies between measurements and results from an accurate model just because the measured and modeled situations are not identical.

1.4 Overview of the thesis

Chapter 2 gives a short introduction to MR safety whereas magnetic tracking is introduced in chapter 3. The aims of this work are presented in chapter 4.

Part II includes papers **I** and **II** on MR-induced pacemaker lead heating and paper **III** on sensor position optimization in magnetic tracking. The technical reports (papers **II** and **III**) will constitute the basis for two journal articles to be submitted.

Chapter 2

Pacemaker lead heating during MRI

Under controlled circumstances, the electromagnetic fields present in MRI are not dangerous for humans. However, interaction of the fields with non-biological objects inside or outside the human body can yield dangerous results. In section 2.1, safety aspects of the three types of fields in MRI are presented. MR safety of pacemaker systems is discussed in section 2.2 and the topic of papers **I** and **II**, pacemaker lead heating, is covered in section 2.3.

2.1 Introduction to MR safety

Below, possible interactions with the human body and objects are summarized for the three types of fields present in MRI: (i) the static field, (ii) the gradient fields, and (iii) the RF field. A more comprehensive summary is available in the work by Nyenhuis et al. [7]. In the following, we consider a system with a cylindrical bore.

2.1.1 Static field

The strength of the static, or B_0, field is the main characteristic of an MRI system. In clinics, 1.5 T and 3 T systems are predominant. The static field is directed along the symmetry axis of the cylindrical bore and it is highly uniform at the mid-point of the bore. Close to the bore openings and outside of the bore, the field strength decays rapidly.

The static field mainly interacts with objects through torques and forces. The magnetic torque will tend to turn an object in such a way that its magnetization is parallel to the static field. Magnetic forces are present where the field varies in space and are thus strongest at the bore openings. These forces can turn an object into a projectile that is drawn towards the

MRI machine. This can result in objects getting stuck to the MRI machine, see the web page [8] for examples such as chairs, gurneys etc. More severely, the flying object can hit and injure staff or patients. A tragic example of this is that of a 6-year-old boy who was killed by trauma to the head from an oxygen tank that was pulled out of the hands of a staff member and subsequently flew into the bore, as described in references [9, 10].

Since both torques and forces are stronger for magnetic than non-magnetic materials, magnetic materials are avoided in pacemaker systems. Such a design change may not be feasible for other types of implants. Magnetic materials are, for example, a crucial component of the transducer in an implantable bone-anchored hearing aid.

2.1.2 Gradient fields

The three gradient fields in MRI operate in the kHz range wherefore their strength needs to be limited in order to avoid undesired nerve stimulation. However, the presence of metallic implants may lead to concentration of the induced currents which can stimulate nerves, e.g. the heart can be stimulated by induced currents on a pacemaker lead.

In addition, since the gradient fields change with time they can cause metallic objects, such as wire loops, to vibrate and thereby create strong acoustic noise. The gradient fields can also couple to active medical implants and cause device malfunction.

2.1.3 RF field

The RF field operates at a frequency of $42.58B_0$ MHz which for a 1.5 T system corresponds to 63.87 MHz. The RF field causes heating of the tissue in the body and its power is therefore limited. The power absorbed by the body is measured in W/kg with the specific absorption rate (SAR) defined by

$$\mathrm{SAR} = \frac{1}{2}\int_{\Omega} \frac{\sigma(\vec{r})|\mathbf{E}(\vec{r})|^2}{\rho(\vec{r})}\, d\Omega \tag{2.1}$$

where σ is the electric conductivity of the tissue, $\mathbf{E}$ is the electric field phasor, ρ is the density of the tissue, $\vec{r}$ is the position vector, and Ω the region of tissue over which the quantities are averaged. Several standards exist which dictates SAR limits. Some of the limits set by these standards are summarized in table 2 of reference [11].

Conducting objects, such as implants and catheters, can increase the local heating. In essence, currents are induced on the object and charge is accumulated near sharp edges and corners, in particular. In the vicinity of the accumulated charge, strong electric fields heat the tissue by Joule heating. In particular, severe heating can occur at the ends of elongated implants such as DBS and pacemaker leads, which is treated in section 2.3 below. A review of heating caused by passive implants is given by Virtanen et al. [12].

2.2 Pacemaker safety in MRI

Pacemaker safety in MRI is of increasing concern to healthcare professionals. In 2007, Martin et al. [13] stated that over 35 million MR studies were performed yearly. At the same time, pacemakers and other active implantable medical devices are used with increased frequency. These two effects lead Kalin et al. [14], who represent Medtronic which is one of the world's largest manufacturers of implantable cardiac devices, to estimate a "$50 - 75$ *% probability of a patient being indicated for an MRI over the lifetime of their* [implantable cardiac] *device*". However, these types of implants are currently contraindicated for MRI, i.e. patients with such an implant are not allowed to be examined with MRI.

2.2.1 Case reports on deaths

Case reports on deaths are hard to find. Martin et al. [13] stated that "*To date* [2007]*, there have been at least 17 pacemaker patient deaths worldwide thought to be attributable to MRI*" without giving any references. More reliable information is given by Gimbel et al. [15] from 1995 who performed a survey where 194 cardiologists and radiologists were asked on MRI examinations of pacemaker (PM) patients. In total 20 scans had been performed on 19 pacemaker patients. A majority of the patients were not affected by the scan but "*One unmonitored PM patient died who was inadvertently scanned*".

Martin et al. [13] continue: "*However, importantly, no deaths have occurred during appropriate physician-supervised monitoring.* In a recent study by Zikria et al. [16] published in 2011, the authors review the medical literature on this topic. In total, 1419 MRI examinations are summarized by the review, from where the authors conclude that "*The data are heterogeneous with regard to MRI being considered for patients with pacemakers, and the benefits of the imaging should outweigh the risks*".

2.2.2 MR safe pacemaker design

Even though the medical community is starting to question the contraindication of pacemakers for MRI, there are still risks wherefore Martin et al. [13] states that "*The ideal solution would be for manufacturers to develop truly MR-compatible devices, so that patients in need of important diagnostic MRI information are not denied*". With the aim of satisfying this need, there are two pacemaker systems available on the market today, which are conditionally safe in MRI. The Medtronic system [17] was introduced in 2008 on the European market and in 2011 on the American market. St. Jude introduced their system [18] on the European market in 2011. To this date it has not been introduced to the American market. Parts of the conditions and dimensions of both systems are summarized in table 2.1. As can be seen in the table, both systems are only allowed for use in 1.5 T systems. The Medtronic system excludes a large part of the torso from examination (the landmark is the isocentre of the bore where the center of the imaging domain is situated). This exclusion serves to reduce the power of the electric field that couples to the lead, which is clearly illustrated by the measurements performed by Nordbeck et al. [19]. In contrast, the restriction on landmark position is not present for the St. Jude system. Furthermore, the Medtronic system limits the SAR, which in turn limits the signal-to-noise ratio and therefore the image quality. Note that 4 W/kg is the standard limit for MRI. Both leads are slightly thicker than the 6 Fr of standard leads.

	Medtronic [17]	St Jude [18]
MRI system	1.5 T only	1.5 T only
Landmark	Outside the zone from vertebra C1 to T12 (approx. nose to lower limit of the rib cage)	No limitation
SAR (whole-body)	$\leq$ 2.0 W/kg	$\leq$ 4.0 W/kg
Lead diameter	7 Fr	Tip 8 Fr Body 6.6 Fr

Table 2.1: Conditions and dimensions for clinically available MR conditional pacemaker systems. (1 Fr = 1/3 mm)

Clearly, improvements in the design of MR safe pacemaker systems are desirable wherefore the topic is interesting to study. In addition, there are still numerous unsolved issues related to the lead heating phenomenon.

2.3 Pacemaker lead heating

The most important adverse effect on pacemaker systems subject to an MRI scan is heating at the lead tip, as concluded by Götte et al. [20] in their review of the current knowledge on pacemakers and internal cardioverter-defibrillators (ICDs) in MRI: "*Currently, lead heating and its related consequences including the formation of oedema and/or loss of capture, seems to be a larger problem than the device functioning in an MR environment. Therefore, pacemaker/ICD patients cannot undergo an MRI scan safely and on a routine basis until the problem of lead heating is resolved*". Heating of pacemaker leads in MRI is caused by the RF field, as stated in section 2.1.3 above.

2.3.1 Mechanism

The incident electric field induces a current in the lead, charge is accumulated at the lead electrodes, and strong electric fields arise in the vicinity of the electrodes. Neufeld et al. [21] and Nordbeck et al. [22] claim that for a lead without loops, this is mainly caused by the part of the incident electric field which is tangential to the lead along its length. A smaller area and sharper end of an electrode results in a stronger electric field wherefore an active fixation (shaped as a corkscrew that is screwed into the heart wall) will create stronger fields than a passive fixation (almost shaped as a half-sphere) for the same accumulated charge. Confer with the limiting case of a sharp cone as presented in reference [23]. The electric field drives currents in the conducting medium that surrounds the electrode which is subsequently heated by Joule heating.

Neufeld et al. [21] state: "*The distribution of the energy deposition at the lead tip is mainly determined by the geometry and the materials of the tip (quasi-static), whereas the energy picked up by the lead is a function of the EM properties (full-wave) of the lead and its length.*

The heating can be quite substantial: Luechinger et al. [24] measured a temperature increase of 20 °C *in vivo* (pigs) whereas Achenbach et al. [25] obtained an increase of 63.1 °C *in vitro* in a somewhat unrealistic worst-case scenario.

2.3.2 Influencing factors

The heating is influenced by numerous factors [26, 27, 28, 29], including:

- RF field strength and frequency

- Type of imaging system (coil design, open or closed bore)
- Type of imaging sequence
- Duration of imaging procedure
- Lead design
- Lead length
- Pacemaker position and lead orientation within the patient
- Lead attached to pacemaker unit or abandoned
- Patient position in the RF coil
- Patient characteristics (size etc.)
- Body structure being imaged
- Type of medical device (pacemaker, ICD)
- Respiratory phase

The heating is highly sensitive to almost all of these factors. For example, Mattei et al. [29] investigated 374 implant configurations experimentally by measuring the heating near the lead tip and concluded that the heating is highly sensitive to the lead configuration. Nordbeck et al. [30], who measured the induced current in the lead for 720 implant configurations in a phantom, also came to the conclusion that the heating is highly sensitive to the implant configuration. This can also be understood by examining the measurements performed by Nordbeck et al. [19, 22] of the electric field inside a standard phantom.

2.3.3 Impact of design parameters

Numerous studies, based on experiments and/or modeling, of how the heating is affected by changes in lead design parameters are available in the literature. The main conclusions from the studies by Nyenhuis et al. [7], Langman et al. [27], Bottomley et al. [28], Yeung et al. [31], Park et al. [32], Mattei et al. [33], Yeung et al. [34], Armenean et al. [35], and Park [36] are summarized below. In all of these studies, the lead is surrounded by a finite or infinite lossy dielectric unless stated otherwise. It should also be noted that in all of the aforementioned studies where modeling has been used, the electrode surfaces have been modeled in such a way that the coupling to the surrounding medium is purely capacitive.

Lead length Yeung et al. [31] described the role of the lead length as follows. The currents induced in a lead by external excitations on different parts of the lead will interfere with each other at the lead tip. For a uniform excitation of a straight bare wire, this interference will be constructive for wires shorter than $\lambda/2$ where λ is the wavelength in the surrounding medium. However, longer wires will experience interference that also contains destructive parts and, therefore, the heating will display a maximum for a certain wire length. This wire length is commonly referred to as the resonance or resonant length. By considering a worst-case excitation where the phase is such that all interference at the tip is constructive, Yeung et al. concluded that "*shorter wires are intrinsically safer than longer ones*".

The same argument was also used by Park et al. [32] to simulate worst case heating. Bottomley et al. [28] folded back a part of a straight lead along itself and showed that this could dramatically increase the heating from long leads that only showed modest heating in a straight configuration.

It must be stressed that for leads which consist of more than a straight wire, the resonant length does not only depend on the wavelength of the RF field in the surrounding medium. Or, as stated by Park et al. [32]: "*The so-called resonant length is thus a function of the construction methodology of a medical lead and can not simply be assumed to be one-half of the RF wavelength in the body*". This was also concluded by, among others, Mattei et al. [33] and is discussed further below.

Lead diameter Yeung et al. [34] modeled straight wires in an infinite homogeneous medium that were excited by a uniform excitation along the wire. By increasing the wire diameter, the heating at the wire end was reduced but there was no change in resonance length. This was confirmed by Armenean et al. [35] who performed measurements of the heating near the end of a straight wire in air with its end inserted in a dielectric material.

Bottomley et al. [28] argued that a larger lead diameter for leads with helical conductors could reduce the heating by means of allowing for smaller pitch angles.

Insulation Park [36] simulated straight wires with bare ends and found that an increase in insulation thickness resulted in longer resonance lengths and increased heating at the lead tip. Similar results were obtained from the simulation and measurements of straight leads by Bottomley et al. [28] who also stated that an increase in insulation thickness not only increased the heating at the lead electrodes but also reduced it along the lead.

Yeung et al. [34] performed simulations of straight wires in an infinite homogeneous medium. The wires were completely insulated, i.e. they had no bare electrodes. By increasing the permittivity of the insulation, they found that the resonance length was reduced and that the heating was slightly reduced. Similar results were obtained by Park [36] for straight wires with bare ends. Nyenhuis et al. [7] explained this as follows: The insulation permittivity is largely inferior to the permittivity of the surrounding tissue and $\lambda \propto 1/\sqrt{\varepsilon_r}$ where ε_r is the relative permittivity of the medium. An increase in insulation permittivity or a decrease in insulation thickness will lead to an increased apparent permittivity around the wire. Thus, the resonance length is decreased.

Fixation modality Mattei et al. [33] performed heating measurements *in vitro* on 30 clinical leads from different manufacturers. The standard ASTM phantom with a straight lead was used as well as an human-shaped phantom with two clinical lead paths, one with the pacemaker in the left pectoral region and one with the pacemaker in the right pectoral region. In addition, for each pacemaker position the lead path ended in either the atrium or the ventricle. Leads with active fixation (metal corkscrew) were found to generate significant higher heating than the leads with passive fixation (rounded tip and tines). The difference was shown to be statistically significant for the SAR but not for the temperature. However, several leads with active fixation heated less than some leads with passive fixation so the trend is strong but not absolute.

Number of conductors From their *in vitro* measurements on 30 clinical leads, Mattei et al. [33] found that bipolar leads (two conductors) heated more than unipolar leads (one conductor) although the difference was statistically significant only for ventricular implants. They also found that for some bipolar leads, and notably two of the three examined ICD leads, heating was more important at the ring electrode than at the tip electrode.

Number of filars Bottomley et al. [28] argued that a higher number of filars would generate more heat due to the associated increase in pitch angle, which is due to physical constraints.

As stated on the Medtronic webpage [37], a reduction from four to two filars in the inner conductor rendered a standard lead conditionally MR safe. In addition, the wire and helix diameters of the inner conductor were increased slightly to ensure proper torque transfer to the active fixation of the lead.

Tip area Mattei et al. [33] could not establish any relation between tip area and SAR from their *in vitro* measurements on 30 clinical leads.

Lead impedance Bottomley et al. [28] concluded from measurements and simulations that an increased total lead impedance reduces the heating ΔT at the lead electrodes. They also established the relation $\Delta T \propto R^{-2}$ by measurements on a straight lead, where R is the total lead resistance.

Along the same line, the highest SAR measured by Mattei et al. [33] was obtained for some of the leads in the study with lowest tip resistance. However, there were also leads with similar tip resistance that generated among the lowest SAR values of the study.

Termination Langman et al. [27] measured heating of active fixation, bipolar pacemaker leads of different lengths in a cylindrical phantom designed to generate a uniform excitation along the lead. The leads were either attached to a pacemaker, capped with a plastic cap or abandoned in the phantom gel. Thus, the two conductors were connected through the electronics of the pacemaker, a short circuit, or the dielectric gel respectively. For clinical lead lengths ($40 - 60\,\text{cm}$), the abandoned leads showed greater lead tip heating than the pacemaker-attached leads.

Mattei et al. [33] stated that their results were in agreement with the findings of Langman et al.

Helix winding and pitch angle Bottomley et al. [28] performed simulations and measurements on leads with one helix-shaped conductor. For straight leads, they found that the heating decreases, in general, when the pitch angle decreases and they explained this by the associated increase in lead inductance. However, there are results from their measurements that do not adhere to this behavior. Furthermore, a triple-layer coaxial lead was tested and showed significant heating. Bottomley et al. concluded by stating: "*piling on windings is no guarantee of MRI safety*".

By dividing the lead in short triple-layer segments, Bottomley et al. created leads with four filars that did not heat more than 1 °C in either straight or fold-back configurations.

2.3.4 Measurements and countermeasures

Heating measurements are usually performed with fluoroptic temperature probes in a phantom filled with a gelled saline. The test standard ASTM

F2182-09 [38] summarizes the main results regarding experimental procedures available in the literature. The strong electric fields are highly localized as discussed above. Although the resulting heating has a much smoother appearance in space than the electric fields, great care must be taken when positioning the temperature probes as shown by Triventi et al. [39] and Mattei et al. [40].

To counteract excessive heating several techniques have been suggested. Bottomley et al. [28] proposed intricate winding schemes for the lead conductors and also listed previously proposed solutions. In the available clinical systems the number of filaments in the inner conductor was reduced in the Medtronic system [17] from 4 to 2. The design solution used in the St. Jude system [18] is not publicly available.

A technique to reduce the heating without altering the lead design was proposed by Eryaman et al. [41] whose idea was to reduce the electric field strength along the lead path by modifying the feeding of the RF coil. Furthermore, Overall et al. [42] exploited the fact that there is no magnetic resonance excitation if the polarization of the RF signal is reversed whereas the induced currents in an elongated implant does not depend on this polarization. Based on this, a technique for estimating the heating potential was proposed by performing a low-power pre-scan of the patient exploiting an RF field with reverse polarization. However, Eryaman et al. [43] commented on a special case where the method proposed by Overall et al. did not work efficiently, i.e. the induced current in the lead differed substantially between the forward and the reverse polarization.

Chapter 3

Optimization of sensor positions in magnetic tracking

3.1 Biomedical applications of magnetic tracking

Magnetic tracking systems determine the position and/or orientation of a device based on its interaction with low-frequency or static magnetic fields. Since the human body is transparent to these fields, magnetic tracking systems do not suffer from interference by the human body, nor do they need to consider variations between patients. Therefore, magnetic tracking systems are attractive for biomedical applications. For example, Plotkin et al. [44] used a magnetic tracking system for eye tracking in order to diagnose Ménière's disease, Yang et al. [45] exploited magnetic tracking for the tracking of a wireless capsule endoscope in the gastro-intestinal tract, and Biosense Webster [46] sells a catheter tracking system based on magnetic tracking.

In this thesis, we focus on the magnetic tracking system described by Iustin et al. [47], which is used for real-time organ-positioning during radiotherapy of prostate cancer tumors. The prostate is continuously changing position within the body due to contractions of the breathing muscles, bowel movements etc. Therefore, a margin of healthy tissue surrounding the tumor is irradiated to ensure that the entire tumor is treated. If the tumor position was known exactly in real-time, the radiation dose could be increased which could result in a shorter, more efficient treatment with less side-effects. The positioning system consists of a transmitter that is implanted near the tumor, an external sensor array, and a data processing unit.

3.2 Positioning procedure

In general, magnetic tracking systems estimate the unknown parameters $\mathbf{p} \in \mathbb{R}^p$ of the tracked device (position and/or orientation) by minimizing the misfit between the values measured by the system $\mathbf{f}^{\text{meas}}$ and the values obtained from a model of the system $\mathbf{f}^{\text{model}}(\mathbf{p})$ by varying $\mathbf{p}$ in an organized way. That is, the optimization problem

$$\underset{\mathbf{p}}{\text{minimize}} \quad J[\mathbf{f}^{\text{meas}}, \mathbf{f}^{\text{model}}(\mathbf{p})] \tag{3.1}$$

is solved for $\mathbf{p}$ where J is a cost function(-al) that quantifies the difference between its arguments. For example, the system presented by Plotkin et al. [44] exploits a system model based on the Biot-Savart law and the Levenberg-Marquardt algorithm for the solution of the optimization problem whereas Paperno et al. [48] modeled the coils in the system by magnetic dipoles. In contrast, Iustin et al. [47] exploited a surrogate model based on measurements as system model.

3.3 Optimization of sensor positions

The performance of a measurement system can be improved by the addition of additional sensors. However, this can be prevented by the associated increase in system cost, longer data processing times, and physical constraints. Therefore, it is important to collect as much information as possible with the available sensors. The sensors' positions constitute one important factor when the maximization of collected information is sought.

3.3.1 Performance measures

A prerequisite for sensor position optimization is the ability to quantify the performance of the system. In general, magnetic tracking systems are modeled with models that are non-linear in the transmitter coordinates. A first order approximation of the impact of measurement noise can be obtained by linearizing the system model around a point of interest $\mathbf{p}_0$. If the gradient $\nabla_{\mathbf{p}} \mathbf{f}^{\text{model}}(\mathbf{p}_0)$ is small (in some sense), the measured value hardly changes when $\mathbf{p}$ changes. Conversely, measurement noise can change the measured signal quite substantially and will thereby cause a large error in the estimated parameters. Therefore, a sensitive measurement system is characterized by large values (in some sense) of the gradient $\nabla_{\mathbf{p}} \mathbf{f}^{\text{model}}(\mathbf{p}_0)$. Thus, the measurement system is sensitive to changes in $\mathbf{p}$ and robust to measurement noise.

Assume that we have N^{rec} sensors, let $\mathbf{V}(\mathbf{p}_0) = \mathbf{f}^{\text{model}}(\mathbf{p}_0) \in \mathbb{R}^{N^{\text{rec}}}$, and let $\mathbf{G} \in \mathbb{R}^{N^{\text{rec}} \times p}$ denote the sensitivity matrix

$$\nabla_{\mathbf{p}} \mathbf{V}(\mathbf{p}_0) = \mathbf{G} = \begin{bmatrix} \nabla_{\mathbf{p}} V_1(\mathbf{p}_0)^T \\ \nabla_{\mathbf{p}} V_2(\mathbf{p}_0)^T \\ \vdots \\ \nabla_{\mathbf{p}} V_{N^{\text{rec}}}(\mathbf{p}_0)^T \end{bmatrix} \tag{3.2}$$

where $\mathbf{a}^T$ denotes the transpose of $\mathbf{a}$. If the measurement noise is Gaussian and independent between the measurements, the uncertainty of the estimated parameters is governed by the so-called Fisher information matrix

$$\begin{aligned} \mathbf{M} = \mathbf{G}^T \mathbf{G} = \sum_{i=1}^{N^{\text{rec}}} \mathbf{M}_i = & \\ = \sum_{i=1}^{N^{\text{rec}}} & \begin{bmatrix} \left(\frac{\partial V_i}{\partial p_1}\right)^2 & \left(\frac{\partial V_i}{\partial p_1}\right)\left(\frac{\partial V_i}{\partial p_2}\right) & \cdots & \left(\frac{\partial V_i}{\partial p_1}\right)\left(\frac{\partial V_i}{\partial p_p}\right) \\ \vdots & & & \vdots \\ \left(\frac{\partial V_i}{\partial p_p}\right)\left(\frac{\partial V_i}{\partial p_1}\right) & \left(\frac{\partial V_i}{\partial p_p}\right)\left(\frac{\partial V_i}{\partial p_2}\right) & \cdots & \left(\frac{\partial V_i}{\partial p_p}\right)^2 \end{bmatrix} \end{aligned} \tag{3.3}$$

where $\mathbf{p_0} = [p_1,\, p_2,\, \ldots,\, p_p]^T$. This follows from the Cramér-Rao inequality, see [49],

$$\operatorname{cov} \hat{\mathbf{p}} \succeq \mathbf{M}^{-1} \tag{3.4}$$

which gives a lower bound[1] for the covariance of the estimated parameter $\hat{\mathbf{p}}$ for an unbiased estimator. For a certain noise level c, the quadratic form $\{\mathbf{x}^T \mathbf{M}^{-1} \mathbf{x} : ||\mathbf{x}|| = c\}$ describes an uncertainty ellipsoid in the parameter space centered around the true value.

The Fisher information matrix $\mathbf{M}$ depends on the sensor positions via the system model $\mathbf{V}$. An optimization problem for the sensor positions can now be formulated: maximize (in some sense) $\mathbf{M}$ by changing the sensor positions. The crucial term here is *in some sense*. Usually, a real-valued function $\Psi(\mathbf{M})$ is maximized. There are a multitude of such functions in the literature, see for example Ucinski [50] and Atkinson et al. [51].

The information above belongs to the field of optimal measurements. Apart from the references given above, more information on this topic can be found in the monograph by Pukelsheim [52] as well as in paper **III**.

---

[1] The notation $\mathbf{A} \succeq \mathbf{B}$ denotes that $\mathbf{A} - \mathbf{B}$ is positive semi-definite.

3.3.2 Example problem

The magnetic flux density $\vec{B}$ from a magnetic dipole with magnetic moment $\vec{m}$ in free space is given by [53]

$$\vec{B} = \frac{\mu_0 m}{4\pi R^3}\left(\hat{R}\, 2\cos\theta + \hat{\theta}\sin\theta\right) \tag{3.5}$$

where μ_0 is the permeability of free space, m is the value of $\vec{m}$, $\vec{R}$ is distance vector from the dipole to the field evaluation point, θ is the angle between $\hat{m}$ and $\vec{R}$, and hats denote unitary vectors.

Now, consider a simplified setting where we only consider the xz-plane. Let a transmitting coil modeled by a magnetic dipole be situated at $(0, 0, z_{\text{trans}})$. Furthermore, let its magnetic moment $\vec{m}_{\text{trans}}$ make an angle θ_{trans} to the positive z-axis such that $\vec{m}_{\text{trans}}$ is parallel to $\hat{z}$ when $\theta_{\text{trans}} = 0$ and parallel to $\hat{x}$ when $\theta_{\text{trans}} = \pi/2$.

From equation 3.5 we can now obtain the expression for the magnetic flux density in a point $\vec{R}_{\text{rec}} = (x_{\text{rec}}, 0, z_{\text{rec}})$ as

$$\begin{aligned}\vec{B}(\vec{R}_{\text{rec}}) = \frac{\mu_0 m}{4\pi R^5}\Bigg[&\hat{x}\Big(2x_{\text{rec}}^2\sin\theta_{\text{trans}} + 3x_{\text{rec}}(z_{\text{rec}} - z_{\text{trans}})\cos\theta_{\text{trans}} \\ &- (z_{\text{rec}} - z_{\text{trans}})^2\sin\theta_{\text{trans}}\Big) \\ &+ \hat{z}\Big(2(z_{\text{rec}} - z_{\text{trans}})^2\cos\theta_{\text{trans}} + 3x_{\text{rec}}(z_{\text{rec}} - z_{\text{trans}})\sin\theta_{\text{trans}} \\ &- x_{\text{rec}}^2\cos\theta_{\text{trans}}\Big)\Bigg]\end{aligned} \tag{3.6}$$

where $R = [x_{\text{rec}}^2 + (z_{\text{rec}} - z_{\text{trans}})^2]^{1/2}$. For a coil positioned at $\vec{R}_{\text{rec}}$ with radius a_{rec}, N_{turns} turns, and magnetic moment parallel to $\hat{z}$, the induced voltage is

$$V = -j\omega\Phi = -j\omega\pi a_{\text{rec}}^2 N_{\text{turns}}\vec{B}(\vec{R}_{\text{rec}})\cdot\hat{z} \tag{3.7}$$

which is equivalent to

$$\begin{aligned}V = -j\omega\pi a_{\text{rec}}^2 N_{\text{turns}}\frac{\mu_0 m}{4\pi R^5}\Big[&2(z_{\text{rec}} - z_{\text{trans}})^2\cos\theta_{\text{trans}} \\ &+ 3x_{\text{rec}}(z_{\text{rec}} - z_{\text{trans}})\sin\theta_{\text{trans}} - x_{\text{rec}}^2\cos\theta_{\text{trans}}\Big].\end{aligned} \tag{3.8}$$

When the derivatives with respect to z_{trans} and θ_{trans} of V have been calculated, the Fisher information matrix can be formed as

$$\mathbf{M} = \sum_{i=1}^{N^{\text{rec}}} \mathbf{M}_i = \sum_{i=1}^{N^{\text{rec}}} \begin{bmatrix} \left(\frac{\partial V_i}{\partial z_{\text{trans}}}\right)^2 & \left(\frac{\partial V_i}{\partial z_{\text{trans}}}\right)\left(\frac{\partial V_i}{\partial \theta_{\text{trans}}}\right) \\ \left(\frac{\partial V_i}{\partial \theta_{\text{trans}}}\right)\left(\frac{\partial V_i}{\partial z_{\text{trans}}}\right) & \left(\frac{\partial V_i}{\partial \theta_{\text{trans}}}\right)^2 \end{bmatrix} \tag{3.9}$$

where each V_i comes with its associated x_{rec}, z_{rec} and R. From equation (3.9), we see that at least two receiving coils are needed to obtain a matrix M with full rank, i.e. we need at least two independent measurements to estimate two parameters.

From equation (3.8), we can compute the positions where the induced voltage in the sensing coil is zero. These positions fulfill

$$\tan\theta_{\text{trans}} = -\frac{1}{3}\left(\frac{2(z_{\text{rec}} - z_{\text{trans}})}{x_{\text{rec}}} - \frac{x_{\text{rec}}}{(z_{\text{rec}} - z_{\text{trans}})}\right). \tag{3.10}$$

The corresponding values of θ_{trans} have been plotted as a function of x_{rec} in figure 3.1 for the case $z_{\text{rec}} = 0$.

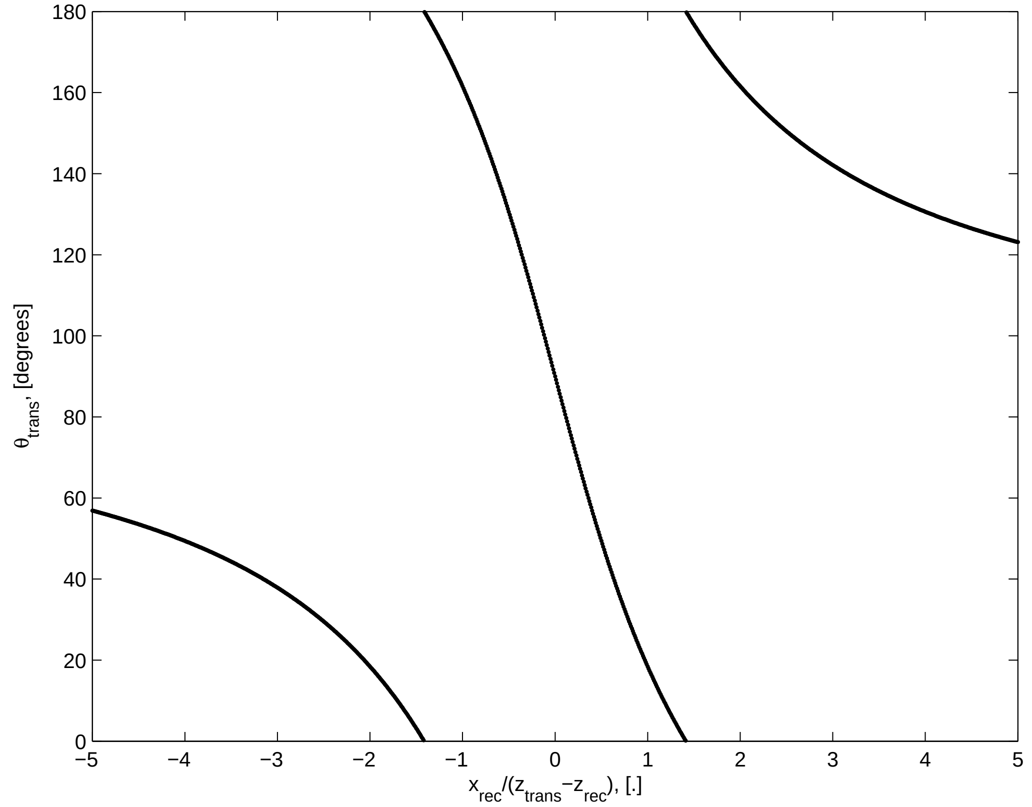

Figure 3.1: Transmitter angles θ_{trans} for which the induced voltage in zero in a receiver coil positioned at $(x_{\text{rec}}, 0, z_{\text{rec}})$ for the case $z_{\text{rec}} = 0$. Note that the x-coordinate of the receiving coil has been normalized with z_{trans}.

Chapter 4

Aim and overview of this work

4.1 Electromagnetic modeling of pacemaker lead heating during MRI

Numerical modeling of pacemaker lead heating during MRI can have several advantages as compared to experiments. Numerical models can take the human body into account, something that is difficult and potentially dangerous to the subject in an experimental setting. Modeling can also provide information which can be difficult to measure, for example the induced currents on the lead. In addition, modeling can prove useful as a tool for lead development as numerous designs can be tested in an automated way without having to be individually constructed. In contrast, extensive measurement campaigns can be both expensive, time-consuming and difficult.

Previous modeling available in literature has focused mainly on the challenges associated with variations between examinations (e.g. Park et al. [54]) and the heterogeneous nature of the human body (e.g. Mattei et al. [55]). The multi-scale part of the problem was addressed by Neufeld et al. [21] who simulated a lead comprising one single helix. However, their choice of FDTD as computational technique limited them from investigating more complex leads at a reasonable computational cost. Nevertheless, modern pacemaker leads are much more complicated than the single-helix model by Neufeld et al. as they often include two conductors consisting of several filars each. As shown by the experiments by Bottomley et al. [28], the lead winding has significant impact on the heating. Thus, the inclusion of fine lead details, such as filars, in the computational models is crucial in order to access the advantages of numerical modeling.

In this work, we develop a computational model for pacemaker lead heating during MRI with the aim of accurately representing the multi-scale part of the problem. The main effort is spent on detailed modeling of the pacemaker lead where the helix-shaped conductors of the lead are modeled with thin-wire segments.

Paper **I** introduces a first version of the model whereas the complete model is presented and exploited in paper **II**. A new meshing scheme for helix-shaped conductors is introduced in paper **I** and its performance is evaluated by means of a convergence study as discussed in section 1.3.4 above. To further analyze the proposed model, paper **II** includes a study on the accuracy of the thin-wire approximation when used to model helix-shaped resonant structures.

One limitation of this work is that the computational results have not been compared to experimental data. As described in section 1.3.4, such a comparison is important and also difficult. Neufeld et al. [21] compared simulation results to measurements from a fully controlled experiment that included a custom made RF coil and very accurate positioning ($< 0.2\,\mathrm{mm}$) of the temperature probes. The simulation results deviated less than the measurement uncertainty of $17\,\%$ from the experimental results.

4.2 Optimization of sensor positions in magnetic tracking

Higher accuracy can in general be achieved by increasing the number of sensors in a measurement system such as a magnetic tracking system. However, constraints in terms of system cost, size, and processing time can limit the number of sensors. Therefore, it is important to maximize the information provided by the sensors. Especially as there are situations where badly placed sensors can render the estimation procedure impossible.

Our overall aim is to optimize the sensor positions of the magnetic tracking system described by Iustin et al. [47]. Previously, Shafrir et al. [56] optimized the sensor positions of a magnetic tracking system designed for tracking of the human eye. The optimization was divided in two steps: one outer and one inner. The outer optimization sought to maximize the performance of the system by changing the sensor positions. The associated cost function was based on the results of the inner optimization. This optimization was designed to find the position within the measurement domain with the worst system performance. For each of the investigated positions in the inner step, 1000 runs of the positioning algorithm was run. As this procedure is time-consuming, there is a need for more elaborate performance measures.

In this work, presented in paper **III**, we use theory from the field of optimal measurements to formulate performance measures that can be used for comparison between different sensor array layouts. A dipole-based model of a generic magnetic tracking system is established and used in conjunction with the performance measures for the optimization of planar sensor arrays.

Bibliography

[1] A Bondeson, T Rylander, and P Ingelström. *Computational electromagnetics.* Texts in applied mathematics. Springer, 2005.

[2] Kane S. Yee. Numerical solution of initial boundary value problems involving Maxwell's equations in isotropic media. *IEEE Transactions on Antennas and Propagation*, 14(3):302–307, May 1966.

[3] A. Taflove. *Computational Electrodynamics: The Finite-Difference Time-Domain Method.* Artech House, Norwood, MA, 1995.

[4] J C Nédélec. Mixed finite elements in $\mathbb{R}^3$. *Numerische Mathematik*, 35(3):315–341, September 1980.

[5] A F Peterson, S L Ray, and R Mittra. *Computational Methods for Electromagnetics.* IEEE Press, New York, NY, 1997.

[6] J. M. Jin. *The Finite Element Method in Electromagnetics.* John Wiley & Sons, New York, NY, 1993.

[7] J.A. Nyenhuis, R. Kamondetdacha, A. Amjad, F.G. Shellock, and A.R. Rezai. MRI and implanted medical devices: basic interactions with an emphasis on heating. *IEEE Transactions on Device and Materials Reliability*, 5(3):467–480, September 2005.

[8] M. NessAiver. Simply Physics - Flying Objects. `www.simplyphysics.com/flying_objects.html`, Accessed Oct. 4, 2011.

[9] Randal C Archibold. Hospital Details Failures Leading to M.R.I. Fatality. `www.nytimes.com/2001/08/22/nyregion/hospital-details-failures-leading-to-mri-fatality.html?src=pm`, Accessed Oct. 4, 2011, Published Aug. 22, 2001.

[10] Mary F Dempsey, Barrie Condon, and Donald M Hadley. MRI safety review. *Seminars in ultrasound, CT, and MR*, 23(5):392–401, October 2002.

[11] J W Hand, Y Li, E L Thomas, M A Rutherford, and J V Hajnal. Prediction of specific absorption rate in mother and fetus associated with MRI examinations during pregnancy. *Magnetic Resonance in Medicine*, 55(4):883–93, 2006.

[12] H. Virtanen, J. Keshvari, and R. Lappalainen. Interaction of Radio Frequency electromagnetic fields and passive metallic implants - a brief review. *Bioelectromagnetics*, 27(6):431–439, 2006.

[13] Edward T Martin and David A Sandler. MRI in patients with cardiac devices. *Current cardiology reports*, 9(1):63–71, March 2007.

[14] Ron Kalin and Marshall S Stanton. Current clinical issues for MRI scanning of pacemaker and defibrillator patients. *Pacing and clinical electrophysiology : PACE*, 28(4):326–8, April 2005.

[15] J. Rod Gimbel, Ronald J. Lorig, and Bruce L. Wilkoff. Safe Magnetic Resonance Imaging of Pacemaker Patients [abstract]. *Journal of the American College of Cardiology*, 25(2):11A, February 1995.

[16] Joseph F Zikria, Stephen Machnicki, Eugene Rhim, Tandeep Bhatti, and Robert E Graham. MRI of patients with cardiac pacemakers: a review of the medical literature. *AJR. American journal of roentgenology*, 196(2):390–401, February 2011.

[17] Medtronic. Revo MRI Pacing System. `www.medtronicexperience.com/ws/files/Client_74/Product_1010/Booth_1022/Module_1054/Asset_163/OverviewBrochure.pdf`, Accessed Oct. 5, 2011.

[18] St. Jude Medical. Tendril MRI Pacing Lead. `www.sjmprofessional.com/Products/Intl/Pacing-Systems/Tendril-MRI-Lead.aspx`, Accessed Oct. 5, 2011.

[19] Peter Nordbeck, Oliver Ritter, Ingo Weiss, Marcus Warmuth, Daniel Gensler, Natalie Burkard, Volker Herold, Peter M Jakob, Georg Ertl, Mark E Ladd, Harald H Quick, and Wolfgang R Bauer. Impact of imaging landmark on the risk of MRI-related heating near implanted medical devices like cardiac pacemaker leads. *Magnetic Resonance in Medicine*, 65(1):44–50, January 2011.

[20] M J W Götte, I K Rüssel, G J de Roest, T Germans, R F Veldkamp, P Knaapen, C P Allaart, and A C van Rossum. Magnetic resonance imaging, pacemakers and implantable cardioverter-defibrillators: current situation and clinical perspective. *Netherlands heart journal*, 18(1):31–7, January 2010.

[21] E Neufeld, S Kühn, G Szekely, and N Kuster. Measurement, simulation and uncertainty assessment of implant heating during MRI. *Physics in medicine and biology*, 54(13):4151–69, July 2009.

[22] Peter Nordbeck, Florian Fidler, Ingo Weiss, Marcus Warmuth, Michael T Friedrich, Philipp Ehses, Wolfgang Geistert, Oliver Ritter, Peter M Jakob, Mark E Ladd, Harald H Quick, and Wolfgang R Bauer. Spatial distribution of RF-induced E-fields and implant heating in MRI. *Magnetic Resonance in Medicine*, 60(2):312–9, 2008.

[23] R. De Smedt. Electric singularity near the tip of a sharp cone. *IEEE Transactions on Antennas and Propagation*, 36(1):152–155, 1988.

[24] R. Luechinger, V.A. Zeijlemaker, E.M. Pedersen, P. Mortensen, E. Falk, F. Duru, R. Candinas, and P. Boesiger. In vivo heating of pacemaker leads during magnetic resonance imaging. *European heart journal*, 26(4):376–383, February 2005.

[25] S. Achenbach, W. Moshage, B. Diem, T. Bieberle, V. Schibgilla, and K. Bachmann. Effects of magnetic resonance imaging on cardiac pacemakers and electrodes. *American Heart Journal*, 134(3):467–473, 1997.

[26] J.L. Helfer. MRI Safety Update: RF Induced Heating. `www.biophan.com/index.php?option=com_docman&task=doc_download&gid=23`, Accessed Oct. 5, 2011, Published 2006.

[27] Deborah A Langman, Ira B Goldberg, J Paul Finn, and Daniel B Ennis. Pacemaker lead tip heating in abandoned and pacemaker-attached leads at 1.5 Tesla MRI. *Journal of Magnetic Resonance Imaging*, 33(2):426–31, February 2011.

[28] Paul A. Bottomley, Ananda Kumar, William A. Edelstein, Justin M. Allen, and Parag V. Karmarkar. Designing passive MRI-safe implantable conducting leads with electrodes. *Medical Physics*, 37(7):3828–3843, 2010.

[29] Eugenio Mattei, Michele Triventi, Giovanni Calcagnini, Federica Censi, Wolfgang Kainz, Gonzalo Mendoza, Howard I Bassen, and Pietro Bartolini. Complexity of MRI induced heating on metallic leads: experimental measurements of 374 configurations. *Biomedical engineering online*, 7(1):11, January 2008.

[30] Peter Nordbeck, Ingo Weiss, Philipp Ehses, Oliver Ritter, Marcus Warmuth, Florian Fidler, Volker Herold, Peter M Jakob, Mark E Ladd, Harald H Quick, and Wolfgang R Bauer. Measuring RF-induced currents inside implants: Impact of device configuration on MRI safety of cardiac pacemaker leads. *Magnetic Resonance in Medicine*, 61(3):570–8, March 2009.

[31] Christopher J Yeung, Robert C Susil, and Ergin Atalar. RF heating due to conductive wires during MRI depends on the phase distribution of the transmit field. *Magnetic Resonance in Medicine*, 48(6):1096–8, December 2002.

[32] S.M. Park, R. Kamondetdacha, and J.A. Nyenhuis. Calculation of MRI-induced heating of an implanted medical lead wire with an electric field transfer function. *Journal of Magnetic Resonance Imaging*, 26(5):1278–1285, 2007.

[33] Eugenio Mattei, Giovanni Calcagnini, Federica Censi, Michele Triventi, and Pietro Bartolini. Role of the lead structure in MRI-induced heating: In vitro measurements on 30 commercial pacemaker/defibrillator leads. *Magnetic Resonance in Medicine*, 000:1–11, July 2011.

[34] C.J. Yeung, R.C. Susil, and Ergin Atalar. RF safety of wires in interventional MRI: using a safety index. *Magnetic Resonance in Medicine*, 47(1):187–193, 2002.

[35] Cristina Armenean, Emmanuel Perrin, Mircea Armenean, Olivier Beuf, Frank Pilleul, and Hervé Saint-Jalmes. RF-induced temperature elevation along metallic wires in clinical magnetic resonance imaging: influence of diameter and length. *Magnetic Resonance in Medicine*, 52(5):1200–6, November 2004.

[36] S.M. Park. *MRI safety: Radiofrequency field induced heating of implanted medical devices.* PhD thesis, Purdue University, West Lafayette, Indiana, USA, 2006.

[37] Medtronic. 5086 MRI Lead Video. `www.medtronicexperience.com/#/us/Revo/Product-Overview/`, Accessed Nov. 3, 2011.

[38] *Standard Test Method for Measurement of Radio Frequency Induced Heating Near Passive Implants During Magnetic Resonance Imaging, Standard F2182-09.* ASTM International, West Conshohocken, PA, USA, 2010.

[39] Michele Triventi, Eugenio Mattei, Giovanni Calcagnini, Federica Censi, Pietro Bartolini, Wolfgang Kainz, and Howard Bassen. Magnetic-resonance-induced heating of implantable leads. *Annali dell'Istituto superiore di sanità*, 43(3):229–40, January 2007.

[40] E Mattei, M Triventi, G Calcagnini, F Censi, W Kainz, H I Bassen, and P Bartolini. Temperature and SAR measurement errors in the evaluation of metallic linear structures heating during MRI using fluoroptic probes. *Physics in medicine and biology*, 52(6):1633–46, March 2007.

[41] Yigitcan Eryaman, Burak Akin, and Ergin Atalar. Reduction of implant RF heating through modification of transmit coil electric field. *Magnetic Resonance in Medicine*, 65(5):1305–13, May 2011.

[42] William R Overall, John M Pauly, Pascal P Stang, and Greig C Scott. Ensuring safety of implanted devices under MRI using reversed RF polarization. *Magnetic Resonance in Medicine*, 64(3):823–33, September 2010.

[43] Yigitcan Eryaman, Sinan Hersek, and Ergin Atalar. Comments on "Ensuring safety of implanted devices under MRI using reversed polarization". *Magnetic Resonance in Medicine*, 000:1–2, October 2011.

[44] A Plotkin, O Shafrir, E Paperno, and D.M. Kaplan. Magnetic eye tracking: A new approach employing a planar transmitter. *IEEE transactions on bio-medical engineering*, 57(5):1209–1215, March 2010.

[45] Wan'an Yang, Chao Hu, Max Q.-H. Meng, Shuang Song, and Houde Dai. A Six-Dimensional Magnetic Localization Algorithm for a Rectangular Magnet Objective Based on a Particle Swarm Optimizer. *IEEE Transactions on Magnetics*, 45(8):3092–3099, August 2009.

[46] Biosense Webster. Carto 3 System. `www.biosensewebster.com/products/navigation/carto3.aspx`, Accessed Oct. 17, 2011.

[47] R. Iustin, J. Linder, E. Isberg, T. Gustafsson, and B. Lennernäs. A Model Based Positioning System. Patent. WO 2008/079071 A1, World Intellectual Property Organization, 2008.

[48] Eugene Paperno and Dmitry Semyonov. A new method for eye location tracking. *IEEE transactions on bio-medical engineering*, 50(10):1174–9, October 2003.

[49] É Walter and L Pronzato. *Identification of parametric models from experimental data.* Communications and control engineering. Springer, 1997.

[50] D Ucinski. *Optimal measurement methods for distributed parameter system identification.* CRC Press LLC, Boca Raton, 2005.

[51] A.C. Atkinson, A.N. Donev, and R. Tobias. *Optimum experimental designs, with SAS*, volume 34. Oxford University Press, USA, 2007.

[52] F Pukelsheim. *Optimal design of experiments.* Classics in applied mathematics. SIAM/Society for Industrial and Applied Mathematics, 2006.

[53] David K. Cheng. *Fundamentals of Engineering Electromagnetics.* Addison-Wesley Publishing Company, 1st edition, 1993.

[54] S.M. Park and M. Conroy. Electromagnetic Modeling of RF Induced Lead Heating - Ensuring MRI for Patients with Active Implanted Medical Devices. In *ISMRM Workshop on MR Safety: RF Heating of the Human in MRI, 2010*, `www.ismrm.org/workshops/Safety_10/program.htm`, Accessed Aug. 22, 2011.

[55] Eugenio Mattei, Giovanni Calcagnini, Federica Censi, Michele Triventi, and Pietro Bartolini. Numerical model for estimating RF-induced heating on a pacemaker implant during MRI: experimental validation. *IEEE transactions on bio-medical engineering*, 57(8):2045–52, August 2010.

[56] Oren Shafrir, Eugene Paperno, and Anton Plotkin. *Magnetic Tracking with a Flat Transmitter.* Lambert Academic Publishing, 2010.